Plasticity of the truth table of low-leakage genetic logic gates

Plasticity of the truth table of low-leakage genetic logic gates

S Smith and R Grima

Abstract

The design and implementation of genetic logic gates is a fundamental component of biological computation. In this article we show that the function of a common class of synthetic genetic AND and NAND gates is not completely dictated by the circuit connectivity, even if promoter leakage is very small. Rather the logic function is strongly determined by a simple power law relationship between the promoter leakage rate and the binding affinity of the protein complex carrying the information from the input to the output of the gate. Depending on the value of the power law exponent, a circuit designed to be an AND gate can actually operate as a TRUE, OR, AND or FALSE gate, even if the leakage rate is practically negligible. Surprisingly all these functionalities are compatible with the physiological range of parameter values showing that the design of genetic logic gates which preserve functionality across cell types and conditions requires careful consideration of both circuit connectivity and parameter values.

I. INTRODUCTION

Analogous to digital Boolean logic gates, genetic logic gates encode logic operations in gene regulatory networks, using protein concentrations as input and output signals [1–3]. Individual logic gates can be used as biosensors, allowing cells to detect and neutralize toxins [4] or pathogens [5]. At a more complex level, several orthogonal logic gates can be combined allowing cells to perform predetermined computations or run simple programs [6, 7]. However there are a number of significant challenges, not least the fact that genetic programs run in the imprecise and constantly changing cellular environment. Consequently, it is essential to understand the robustness of genetic logic gates to the inconvenient realities of cell biology [8].

Previous computational studies have used a combination of deterministic modelling and stochastic simulation techniques to investigate logic gate design [9–12], robustness to noise [10, 13–15], and robustness to varying input concentrations [16]. An important factor which can determine logic gate function is promoter leakage [17], which refers to the fact that promoters are not perfectly efficient and transcribe mRNA at a low rate even when inactive. Inefficiencies of this type have clear implications for genetic logic gates: instead of the ON/OFF states of digital logic, genetic logic instead uses *high*/*low* protein concentrations, and it is easy to see how the distinction between *low* and *high* could become blurred for a leaky system. Hence engineering logic gates with minimal leakage has been one of the goals of various studies [2, 18, 19].

In this article we use rate equations (REs) [20] to derive truth tables for the output of genetic AND and NAND gates with low promoter leakage. In particular, we show that different logic gate functions are intimately related to the value of the exponent characterising the power law relationship between the leakage rate and the binding affinity of the protein complex carrying the information from the input to the output of the gate. Our study thus identifies the optimal parameter relationships leading to a desired gate function and importantly shows that even if leakage is practically negligible, still a network can display logic function which is completely different than the one suggested by the network's connectivity. We also confirm the predictions of our deterministic theory with stochastic simulations of the corresponding logic gates using the Gillespie algorithm [21].

II. RESULTS

A. AND gate

Following the design of Wang et al. [2] we consider a genetic AND gate comprising five proteins - I_1, I_2 (inputs), R_1, R_2 (intermediates), and R_3 (output) - and three promoters - P_1, P_2, and P_3. As shown schematically in Fig. 1, the AND gate operates as follows. Each of the input proteins (I_1, I_2) can activate a promoter (P_1, P_2 respectively), which in turn expresses another protein (R_1, R_2 respectively). These proteins bind to form a complex (R_{12}) which in turn activates a third promoter (P_3) which expresses the output protein (R_3).

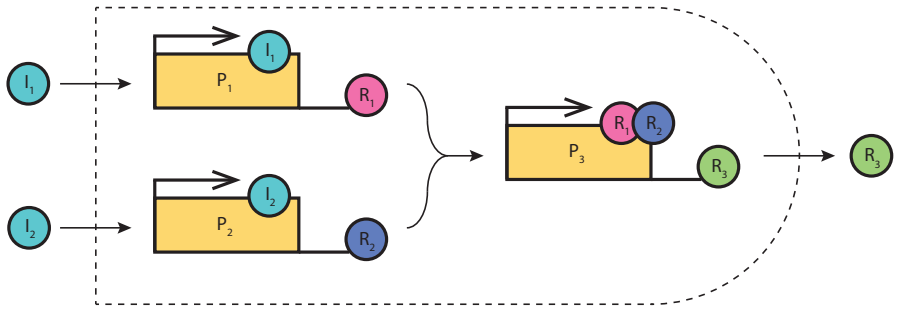

FIG. 1: Diagram of a genetic AND gate. Input proteins I_1 and I_2 bind to promoters P_1 and P_2 respectively, inducing the expression of proteins R_1 and R_2 respectively. These cooperatively bind to a promoter P_3, inducing the expression of the output protein R_3 (color online).

In principle, this system functions as an AND gate. If both input proteins (I_1, I_2) are present in sufficiently high concentrations, then R_1 and R_2 will both be expressed, leading to the formation of the R_{12} complex and the subsequent expression of the output protein R_3. However, if one or both of the inputs is not present (or present in a low concentration), then one or both of the intermediate proteins (R_1, R_2) will be absent, leading to a very low concentration of the complex (R_{12}) and minimal expression of the output R_3.

This system can be mathematically modelled using the REs (see Methods for details). At steady-state, we can write the concentration of the output protein R_3 as:

$$[R_3] = \frac{C_1 C_2 C_3 [I_1] [I_2]}{K_3 K_{12} ([I_1] + K_1) ([I_2] + K_2) + C_1 C_2 [I_1] [I_2]}, \tag{1}$$

where $[I_{1,2}]$ are the concentrations of the input proteins, C_i is the maximum concentration of R_i (at full expression), K_i is the dissociation constant for P_i, and K_{12} is the dissociation

constant for R_{12}. We can write a truth table, analogous to the standard logic gate tables, to determine the function of this system under different input conditions. Table I has the

$[I_1]$	$[I_2]$	$[R_3]$
0	0	0
∞	0	0
0	∞	0
∞	∞	$\frac{C_1C_2C_3}{K_3K_{12}+C_1C_2}$

TABLE I: Truth table for an idealised genetic AND gate with no promoter leakage.

characteristic form of an AND gate truth table, since the outputs are zero except when both inputs are present. Note that the input concentrations range from 0 to ∞: by ∞ we mean a "very high concentration", such that the corresponding promoter is permanently activated. Note also that the output concentration with both inputs on is not equal to C_3. This is because, even with maximal concentations of R_1 and R_2, the complex R_{12} may be present in low concentrations if the dissociation constant K_{12} is large (i.e. if R_1 and R_2 have a low binding affinity). If R_1 and R_2 have a high binding affinity, then K_{12} will be small and $[R_3] \approx C_3$.

We now modify the above expressions to account for the effect of promoter leakage. We model promoter leakage in the following way. Each unit concentration of promoter P_i, whether active or not, expresses protein at a low basal rate l_i. An activated promoter expresses protein at an additional rate t_i, so that the total expression rate will be l_i when inactive and $l_i + t_i$ when active. We define the non-dimensional parameter $\lambda_i = l_i/t_i$ as the *relative leakage* of promoter P_i. $\lambda_i \gg 1$ implies that the leakage is very high, such that an active and inactive P_i will express at roughly the same rate; $\lambda \approx 1$ implies that the leakage is high, such that an active P_i will express at double the rate of an inactive P_i; $\lambda \ll 1$ implies that the leakage is low, so that an inactive P_i expresses at a very low rate compared to an active P_i.

Modifying Eq. (1) to account for leakage (see Methods for details), we get:

$$[R_3] = C_3 \left(\lambda_3 + \frac{C_1C_2 \left(\lambda_1 + \frac{[I_1]}{[I_1]+K_1}\right)\left(\lambda_2 + \frac{[I_2]}{[I_2]+K_2}\right)}{K_3K_{12} + C_1C_2 \left(\lambda_1 + \frac{[I_1]}{[I_1]+K_1}\right)\left(\lambda_2 + \frac{[I_2]}{[I_2]+K_2}\right)} \right). \quad (2)$$

We note that experimentally the leakage parameter λ can typically range from $10^{-3} - 10^{-1}$,

values which are much smaller than one [2]. Hence we use this simplifying assumption in all the calculations that follow. The corresponding truth table with leakage is shown in Table II. We note that all inputs generate *some* non-zero output, and this output is due partly to

$[I_1]$	$[I_2]$	$[R_3]$
0	0	$C_3\left(\lambda_3 + \frac{C_1C_2\lambda_1\lambda_2}{K_3K_{12}+C_1C_2\lambda_1\lambda_2}\right)$
∞	0	$C_3\left(\lambda_3 + \frac{C_1C_2\lambda_2}{K_3K_{12}+C_1C_2\lambda_2}\right)$
0	∞	$C_3\left(\lambda_3 + \frac{C_1C_2\lambda_1}{K_3K_{12}+C_1C_2\lambda_1}\right)$
∞	∞	$C_3\left(\lambda_3 + \frac{C_1C_2}{K_3K_{12}+C_1C_2}\right)$

TABLE II: Truth table for an AND gate with small leakage ($\lambda_i \ll 1$).

leakage in the output promoter P_3, but also due to leakage in the input promoters ($P_1,\ P_2$) inducing normal (non-leaky) expression of R_3. Unlike the non-leaky case displayed in Table I, the function of the leaky AND gate is parameter-dependent.

We define the non-dimensional parameter $\gamma = \frac{K_3K_{12}}{C_1C_2}$, and assume that all three promoters are roughly equally leaky ($\lambda_1 \approx \lambda_2 \approx \lambda_3 = \lambda$). If we define $[R_3]_{I_1,I_2}$ as the concentration of R_3 given the inputs I_1 and I_2 then it is straightforward to show that $[R_3]_{0,0} < [R_3]_{\infty,0} = [R_3]_{0,\infty} < [R_3]_{\infty,\infty}$. Defining $\Delta_1 = ([R_3]_{\infty,0} - [R_3]_{0,0})/C_3$ and $\Delta_2 = ([R_3]_{\infty,\infty} - [R_3]_{\infty,0})/C_3$, using the expressions in Table II we obtain:

$$\Delta_1 \simeq \frac{\gamma\lambda}{(\gamma+\lambda^2)(\gamma+\lambda)}, \tag{3}$$

$$\Delta_2 \simeq \frac{\gamma}{(1+\gamma)(\gamma+\lambda)}. \tag{4}$$

Note that Δ_i is a non-dimensional variable since it is expressed in terms of the non-dimensional parameters γ and λ. OR gate functionality occurs when $[R_3]_{\infty,\infty} \approx [R_3]_{0,\infty} = [R_3]_{\infty,0} \gg [R_3]_{0,0}$ which means Δ_1 should be very large and Δ_2 should be very small. It is optimal when Δ_1 takes its largest possible value of 1 and Δ_2 takes the minimum possible value of zero. By similar reasoning, we find that AND gate functionality occurs when $[R_3]_{\infty,\infty} \gg [R_3]_{0,\infty} = [R_3]_{\infty,0} \approx [R_3]_{0,0}$ which means Δ_1 should be very small and Δ_2 should be very large. It is optimal when Δ_1 takes its minimum possible value of 0 and Δ_2 takes the maximum possible value of 1. A density plot of $\Delta_1 - \Delta_2$ is shown in Fig. 2.

Next we find parameter regimes where these optimal gate behaviour occurs. For a fixed value of the leakage parameter λ, Δ_1 approaches zero as $\gamma \to 0$ and $\gamma \to \infty$ and achieves a

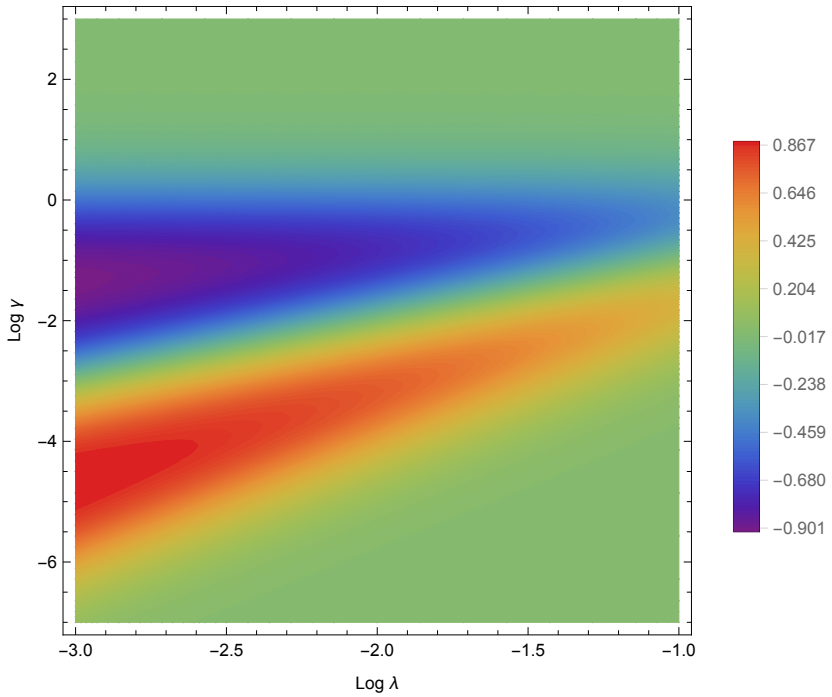

FIG. 2: A density plot of $\Delta_1 - \Delta_2$ as a function of the two non-dimensional parameters λ and γ for the genetic circuit shown in Fig. 1. The (upper) blue-purple region shows the region of parameter space where $\Delta_2 \gg \Delta_1$ implying AND gate behaviour. Contrastingly, the (lower) red-orange region shows the region of parameter space where $\Delta_1 \gg \Delta_2$ implying OR gate behaviour. Note that the log is base 10 (color online).

maximum equal to ≈ 1 when:

$$\gamma = \lambda^{3/2}. \tag{5}$$

The function Δ_2 has similar behaviour however it reaches a maximum equal to ≈ 1 when:

$$\gamma = \sqrt{\lambda}. \tag{6}$$

Furthermore when Δ_1 achieves it maximum of ≈ 1, we find that Δ_2 is equal to $\approx \sqrt{\lambda}$ which is very small since $\lambda \ll 1$ (and viceversa). Thus it follows by our discussion in the previous paragraph that optimal OR and AND gate functionalities are achieved when $\gamma = \lambda^{3/2}$ and $\gamma = \lambda^{1/2}$ respectively. For $\gamma = \lambda$, we find that $\Delta_1 = \Delta_2$ which implies that in this case there are 3 clearly separated output concentrations, i.e., there is no possible interpretation as a high/low output of logic gates and thus the gate behaviour is here undetermined. Fig. 3 shows the variation of the output $[R_3]$ for the four different inputs as a function of the

parameter γ, at fixed value of λ; the values of γ derived above and which give optimal OR and AND gates are shown as vertical lines.

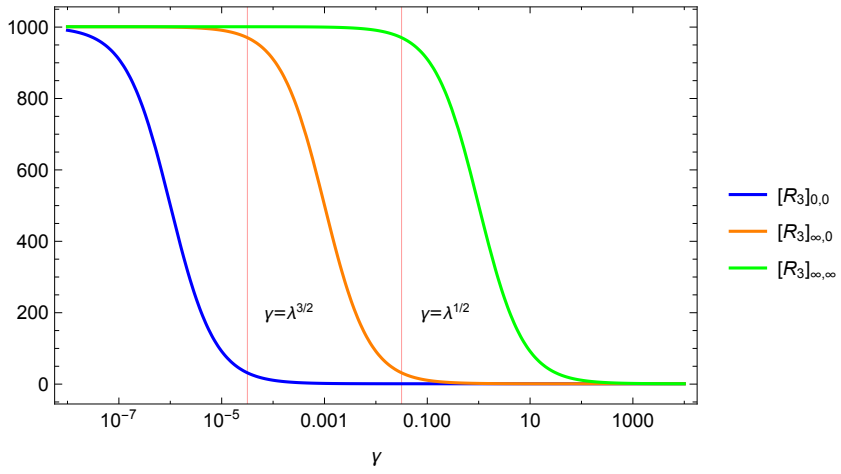

FIG. 3: Plot of the output $[R_3]$ for the four different inputs of the genetic circuit shown in Fig. 1 as a function of the parameter γ. The expressions plotted are shown in Table II. The parameters are $\lambda_1 = \lambda_2 = \lambda_3 = \lambda = 0.001$ and $C_3 = 1000$. The vertical lines $\gamma = \lambda^{3/2}$ and $\gamma = \lambda^{1/2}$ show the parameters leading to optimal OR and AND gate functionality, respectively (color online).

As we decrease γ below the optimal OR value of $\lambda^{3/2}$, we find using the equations in Table II that $[R_3]_{\infty,\infty} \approx [R_3]_{0,\infty} = [R_3]_{\infty,0}$ stay approximately equal to the maximum of C_3 while $[R_3]_{0,0}$ increases from its minimum of $C_3\sqrt{\lambda}$ and approaches C_3 as $\gamma \to 0$ (this can also be seen in Fig. 3). Hence OR gate functionality becomes less pronounced as γ decreases below the value of $\lambda^{3/2}$ and in the limit of very small γ, the gate's function becomes that of a TRUE gate (also known as T or Tautology [22]), which returns a high concentration regardless of input.

As we increase γ above the optimal AND value of $\lambda^{1/2}$, we find using the equations in Table II that $[R_3]_{0,\infty} = [R_3]_{\infty,0} \approx [R_3]_{0,0}$ stay approximately equal to the minimum of $C_3\sqrt{\lambda}$ while $[R_3]_{\infty,\infty}$ decreases from its maximum of C_3 and approaches $C_3\sqrt{\lambda}$ as $\gamma \to \infty$ (this can also be seen in Fig. 3). Hence AND gate functionality becomes less pronounced as γ increases above the value of $\lambda^{1/2}$ and in the limit of very large γ, the gate's function becomes that of a FALSE gate, which returns a low concentration regardless of input. Hence we expect the AND gate output to become highly noisy, as γ increases beyond $\lambda^{1/2}$ since molecular fluctuations tend to increase with decreasing molecule numbers [23].

In summary, the gate's function is determined by simple power law relationships between γ and λ (see Table III).

Case	Regime	Gate functionality
I	$\gamma \gg \sqrt{\lambda}$	noisy AND or FALSE
II	$\gamma \approx \sqrt{\lambda}$	optimal AND
III	$\gamma \approx \lambda$	undetermined
IV	$\gamma \approx \lambda^{3/2}$	optimal OR
V	$\gamma \ll \lambda^{3/2}$	TRUE

TABLE III: Gate functionality as a function of the two non-dimensional parameters γ and λ for the circuit shown in Fig. 1

Next we test whether our deterministic theoretical predictions using stochastic simulations. The reason for doing such a comparison is that stochasticity in molecule numbers plays a large role in determining intracellular dynamics [23] and in some cases stochastic models lead to completely different predictions than REs [24, 25]. In Fig. 4 we compare deterministic theory with stochastic simulations by fixing λ at a low level of leakage, and varying γ. When $\gamma = \lambda^{-1}$, the gate has notional AND functionality in the deterministic model, but the stochastic simulations show that noise is so high as to render the gate essentially useless (Case I in Table III). When $\gamma = \lambda^{1/2}$, our modelling predicts optimal AND functionality, and indeed this is what we see deterministically, and stochastically with relatively low noise (Case II in Table III). Similarly, when $\gamma = \lambda^{3/2}$, our modelling predicts optimal OR functionality, which is confirmed with both deterministic and stochastic simulations (Case IV in Table III). When γ is reduced even further, our modelling predicts that the gate should approach a TRUE gate, which can be seen in the rightmost panels of Fig. 4 (Case V in Table III).

These simulations confirm what our modelling predicted: no matter how low the leakage (λ), there is always only a range of parameter (γ) values for which AND functionality is optimised. Straying too far from the optimal γ risks either having functionality swamped by noise, or else switching to OR-type behaviour.

The relevance of our theory relies on the assumption that γ and λ can be comparable in size for realistic parameter values. In Table VI we display experimentally determined ranges

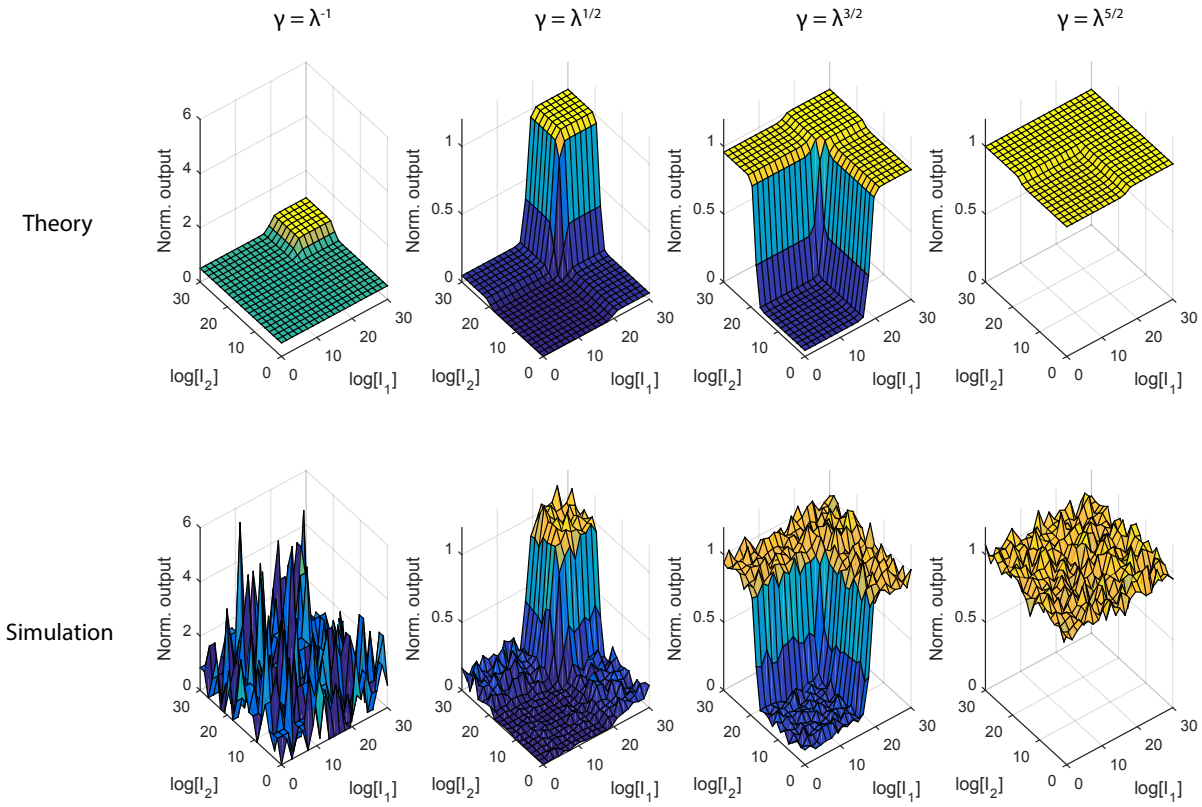

FIG. 4: Surface plots of gate output for the AND gate with varying values of γ, using deterministic theory (Eq. (2)) and stochastic simulations of the gate. The gate functionality shifts from noisy, to AND, to OR, to TRUE as the γ decreases relative to λ which is fixed to 0.002. Other parameter values are given in the Methods section. The log is base 10. Note that the y-axis shows the gate output normalised by the deterministic maximum (color online).

for the relevant parameter values from various sources in the literature, finding that λ can typically range from $10^{-3} - 10^{-1}$, while γ can in principle range widely from $10^{-7} - 10^{10}$. In reality γ will typically be nearer the lower end of this spectrum, because the upper limit of 10^{10} corresponds to the extreme case where the *maximal* concentration of R_1 and R_2 is around $10^{-8}M$ (~ 10 molecules per *E. coli* cell). Using a more conservative (albeit *ad hoc*) assumption that C_i is never less than $10^{-5}M$ ($\sim 10^4$ molecules per *E. coli* cell), γ would range from $10^{-7} - 10^4$. This places the range of λ in the centre of the possible range of γ, implying that all five functionalities listed in Table III are realistically possible.

Parameter	Type	Range	Source
K_i	Promoter dissociation constant	$10^{-9} - 10^{-4} M$	[2]
K_{12}	Protein-protein dissociation constant	$10^{-6} - 10^{-2} M$	[26]
C_i	Maximal protein concentration	$10^{-8} - 10^{-4} M$	[27]
λ_i	Relative leakage	$10^{-3} - 10^{-1}$	[2]
γ	Non-dimensional parameter	$10^{-7} - 10^{10}$	see main text

TABLE IV: Experimentally determined ranges for the AND gate parameters.

B. NAND gate

Next, we study a genetic NAND gate, again following the design of Wang et al. [2]. This gate is constructed by simply appending a NOT gate to the AND gate shown in Fig. 1. An example of a genetic NOT gate is shown in Fig. 5. An input protein R_3 can bind to a promoter P_4, repressing the expression of the output protein R_4. Thus, a high concentration of R_3 should result in a low concentration of R_4, and vice-versa. If the R_3 in Fig. 5 is the same R_3 as that in Fig. 1, then the collective behaviour of the systems is that of a NAND gate.

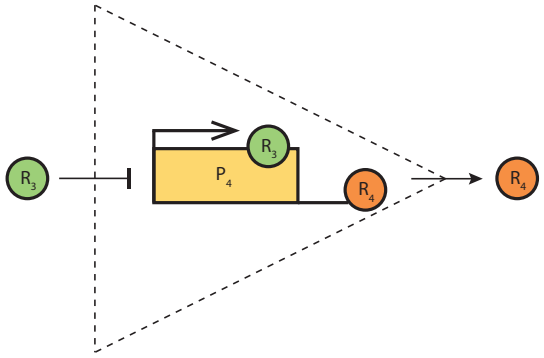

FIG. 5: Diagram of a genetic NOT gate. Input protein R_3 (the output from the AND gate in Fig. 1) binds to promoter P_4, repressing the expression of protein R_4 (color online).

Applying the REs to the updated NAND system, we find that the steady-state concen-

tration of R_4 (the new output protein) is given by:

$$[R_4] = C_4 \left(\lambda_4 + K_4 \left[K_4 + C_3 \left(\lambda_3 + \frac{C_1 C_2 \left(\lambda_1 + \frac{I_1}{I_1+K_1}\right)\left(\lambda_2 + \frac{I_2}{I_2+K_2}\right)}{K_3 K_{12} + C_1 C_2 \left(\lambda_1 + \frac{I_1}{I_1+K_1}\right)\left(\lambda_2 + \frac{I_2}{I_2+K_2}\right)} \right) \right]^{-1} \right), \tag{7}$$

where K_4, C_4, and λ_4 are defined for P_4 analogously to the parameters for the other P_i (see Methods for details). The truth table for the NAND gate (assuming $\lambda_i \ll 1$ for all i) is shown in Table V, for reference we also show the gate function with zero leakage (i.e. $\lambda_1 = \lambda_2 = \lambda_3 = \lambda_4 = \lambda = 0$). We note that, unlike the AND gate, the NAND gate is an imperfect gate even with zero leakage, since some R_4 is expressed even when the output should be zero (when $[I_1] = [I_2] = \infty$). This is because of the parameter K_4, the dissociation constant for the protein R_3 and promoter P_4: if K_4 is large, then P_4 may not be completely bound even when R_3 is maximally expressed, and so the NOT gate will not function perfectly; however, if K_4 is small, then the NOT gate should work well and the NAND output will be close to zero when both inputs are large.

$[I_1]$	$[I_2]$	$[R_4]$	$[R_4]\,\vert_{\lambda=0}$
0	0	$C_4\left(\lambda_4 + K_4\left[K_4 + C_3\left(\lambda_3 + \frac{C_1C_2\lambda_1\lambda_2}{K_3K_{12}+C_1C_2\lambda_1\lambda_2}\right)\right]^{-1}\right)$	C_4
∞	0	$C_4\left(\lambda_4 + K_4\left[K_4 + C_3\left(\lambda_3 + \frac{C_1C_2\lambda_2}{K_3K_{12}+C_1C_2\lambda_2}\right)\right]^{-1}\right)$	C_4
0	∞	$C_4\left(\lambda_4 + K_4\left[K_4 + C_3\left(\lambda_3 + \frac{C_1C_2\lambda_1}{K_3K_{12}+C_1C_2\lambda_1}\right)\right]^{-1}\right)$	C_4
∞	∞	$C_4\left(\lambda_4 + K_4\left[K_4 + C_3\left(\lambda_3 + \frac{C_1C_2}{K_3K_{12}+C_1C_2}\right)\right]^{-1}\right)$	$C_4K_4\left[K_4 + \frac{C_1C_2C_3}{K_3K_{12}+C_1C_2}\right]^{-1}$

TABLE V: Truth table for a NAND gate with and without leakage.

We use the non-dimensional parameter $\gamma = \frac{K_3K_{12}}{C_1C_2}$ previously defined and define a new non-dimensional parameter $\alpha = C_3/K_4$ and assume that all three promoters are roughly equally leaky ($\lambda_1 \approx \lambda_2 \approx \lambda_3 \approx \lambda_4 = \lambda$). It is straightforward to show that $[R_4]_{0,0} > [R_4]_{\infty,0} = [R_4]_{0,\infty} > [R_4]_{\infty,\infty}$. Next we perform a similar analysis as for the AND gate previously and find parameter regimes where different behaviours occur. Defining $\Delta_1 = ([R_4]_{0,0} - [R_4]_{\infty,0})/C_4$ and $\Delta_2 = ([R_4]_{\infty,0} - [R_4]_{\infty,\infty})/C_4$, using the expressions in Table V

we obtain:

$$\Delta_1 \simeq \frac{\alpha\gamma\lambda}{(\gamma+\alpha\gamma\lambda+\lambda^2(1+\alpha))(\gamma+\alpha\gamma\lambda+\lambda(1+\alpha))}, \tag{8}$$

$$\Delta_2 \simeq \frac{\alpha\gamma}{(\gamma+\alpha\gamma\lambda+\lambda(1+\alpha))(\gamma+\alpha(1+\lambda(3+3\lambda+\gamma)))}. \tag{9}$$

Note that Δ_i is a non-dimensional variable since it is expressed in terms of the non-dimensional parameters γ and λ. NOR gate functionality occurs when $[R_4]_{\infty,\infty} \approx [R_4]_{0,\infty} = [R_4]_{\infty,0} \ll [R_4]_{0,0}$ which means Δ_1 should be very large and Δ_2 should be very small. It is optimal when Δ_1 takes its largest possible value of 1 and Δ_2 takes the minimum possible value of zero. By similar reasoning, we find that NAND gate functionality occurs when $[R_4]_{\infty,\infty} \ll [R_4]_{0,\infty} = [R_4]_{\infty,0} \approx [R_4]_{0,0}$ which means Δ_1 should be very small and Δ_2 should be very large. It is optimal when Δ_1 takes its minimum possible value of 0 and Δ_2 takes the maximum possible value of 1.

One can deduce that if the leakage parameter λ is fixed, Δ_1 approaches zero as $\gamma \to 0$ and $\gamma \to \infty$ and achieves a maximum equal to ≈ 1 when:

$$\gamma \approx \lambda, \quad \alpha \approx \lambda^{-1/2}. \tag{10}$$

The function Δ_2 has similar behaviour however it reaches a maximum equal to ≈ 1 when:

$$\gamma \approx 1, \quad \alpha \approx \lambda^{-1/2}. \tag{11}$$

The reasoning behind these conditions is as follows. For general α, the maximum reached by Δ_1 occurs at $\gamma \approx (1+\alpha)\lambda^{3/2}/(1+\alpha\lambda)$ and is equal to $\alpha/(1+\alpha)(1+\alpha\lambda)$. Furthermore the latter expression reaches its maximum value of ≈ 1 when $\alpha \approx \lambda^{-1/2}$; hence follows Eq. (10). Note that the only assumption we have here made is that $\lambda \ll 1$ since this is experimentally justified. By similar arguments for Δ_2, one can obtain Eq. (11).

Furthermore when Δ_1 achieves its maximum, we find that Δ_2 is very small and equal to $\approx \sqrt{\lambda}$ (and viceversa). Thus it follows by our discussion in the previous paragraph that optimal NOR and NAND gate functionalities are achieved when $\gamma \approx \lambda$ and $\gamma \approx 1$, respectively provided that the condition $\alpha \approx \lambda^{-1/2}$ is also fulfilled. For $\gamma \approx \lambda^{1/2}$, we find that $\Delta_1 = \Delta_2$ which implies that in this case there are 3 clearly separated output concentrations, i.e., there is no possible interpretation as a high/low output of logic gates and thus the gate behaviour is here undetermined. Fig. 6 shows the variation of the output $[R_4]$ for the four different inputs as a function of the parameter γ, at fixed value of λ and

$\alpha = \lambda^{1/2}$; the values of γ derived above and which give optimal NOR and NAND gates are shown as vertical lines.

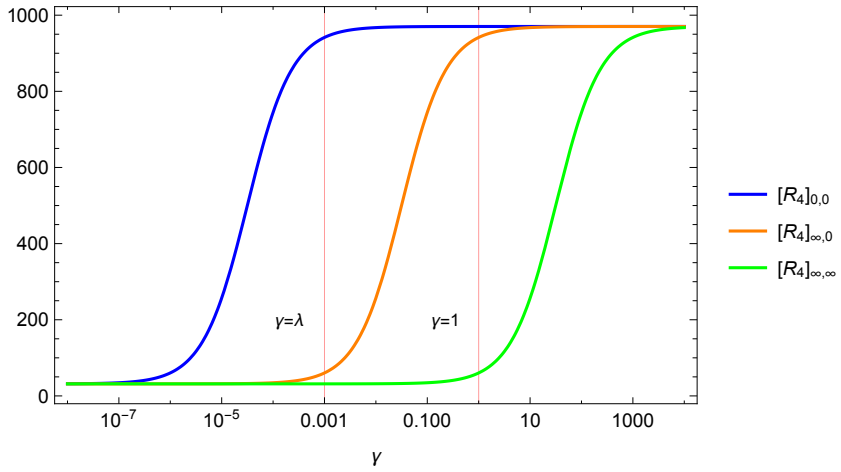

FIG. 6: Plot of the output $[R_4]$ for the four different inputs of the genetic circuit shown in Fig. 5 as a function of the parameter γ. The expressions plotted are shown in Table V (the case of non-zero λ). The parameters are $\lambda_1 = \lambda_2 = \lambda_3 = \lambda_4 = \lambda = 0.001$, $\alpha = \lambda^{-1/2}$ and $C_4 = 1000$. The vertical lines $\gamma = \lambda$ and $\gamma = 1$ show the parameters leading to optimal NOR and NAND gate functionality, respectively (color online).

As we decrease γ below the optimal NOR value of λ, we find using the equations in Table V that $[R_4]_{\infty,\infty} \approx [R_4]_{0,\infty} = [R_4]_{\infty,0}$ stay approximately equal to the minimum of $C_4\sqrt{\lambda}$ while $[R_4]_{0,0}$ decreases from its maximum of C_4 and approaches $C_4\sqrt{\lambda}$ as $\gamma \to 0$ (this can also be seen in Fig. 6). Hence NOR gate functionality becomes less pronounced as γ decreases below the value of λ and in the limit of very small γ, the gate's function becomes that of a FALSE gate, which returns a low concentration regardless of input. Hence we expect the NOR gate output to become highly noisy, as γ approaches zero since molecular fluctuations increase with decreasing molecule numbers.

As we increase γ above the optimal NAND value of 1, we find using the equations in Table V that $[R_4]_{0,\infty} = [R_4]_{\infty,0} \approx [R_4]_{0,0}$ stay approximately equal to the maximum of C_4 while $[R_4]_{\infty,\infty}$ increases from its minimum of $C_4\sqrt{\lambda}$ and approaches C_4 as $\gamma \to \infty$ (this can also be seen in Fig. 6). Hence NAND gate functionality becomes less pronounced as γ increases above the value of 1 and in the limit of very large γ, the gate's function becomes that of a TRUE gate, which returns a high concentration regardless of input.

In summary, the gate's function is determined by simple power law relationships between α, γ and λ (see Table VI).

Case	Regime	Gate functionality
I	$\gamma \gg 1$	TRUE
II	$\gamma \approx 1$	optimal NAND
III	$\gamma \approx \lambda^{1/2}$	undetermined
IV	$\gamma \approx \lambda$	optimal NOR
V	$\gamma \ll \lambda$	noisy NOR or FALSE

TABLE VI: Gate functionality as a function of the two non-dimensional parameters γ and λ for the circuit shown in Fig. 5. Note that in all cases $\alpha \approx \lambda^{-1/2}$ since this value maximises the differences between concentrations representing logic high and low.

To test the prediction of an optimal choice of γ for NAND and NOR functionalities, in Fig. 7 we compare deterministic theory with stochastic simulations, fixing $\lambda = 0.002$ and $\alpha = \lambda^{-1/2}$, and varying γ. When $\gamma = (1+\alpha)\lambda^{-1} \approx \lambda^{-3/2}$, the gate is predicted to have TRUE functionality, which is confirmed in both the deterministic and stochastic simulations. When $\gamma = (1+\alpha)\lambda^{1/2} \approx 1$, our modelling predicts optimal NAND functionality, and indeed this is what we see deterministically, and stochastically with relatively low noise. Similarly, when $\gamma = (1+\alpha)\lambda^{3/2} \approx \lambda$, our modelling predicts optimal NOR functionality, which is confirmed with both deterministic and stochastic simulations. When γ is reduced even further to $\gamma = (1+\alpha)\lambda^{5/2} \approx \lambda^2$ our modelling predicts that the gate functionality should break down due to noise, and this can be seen in the rightmost panels of Fig. 7, where the basal level of expression is high relative to the maximal expression, and noise is starting to swamp any discernible gate-like behaviour.

These simulations again confirm what our theory has predicted: there is only a narrow range of parameter values for which NAND functionality is optimised. Straying too far from these optimal parameters risks either having functionality swamped by noise, or else switching to NOR- or TRUE-type behaviour. The relevance of our theory is that the range of realistic parameter values (as shown in Table IV) are compatible with all five gate functionalities listed in Table VI.

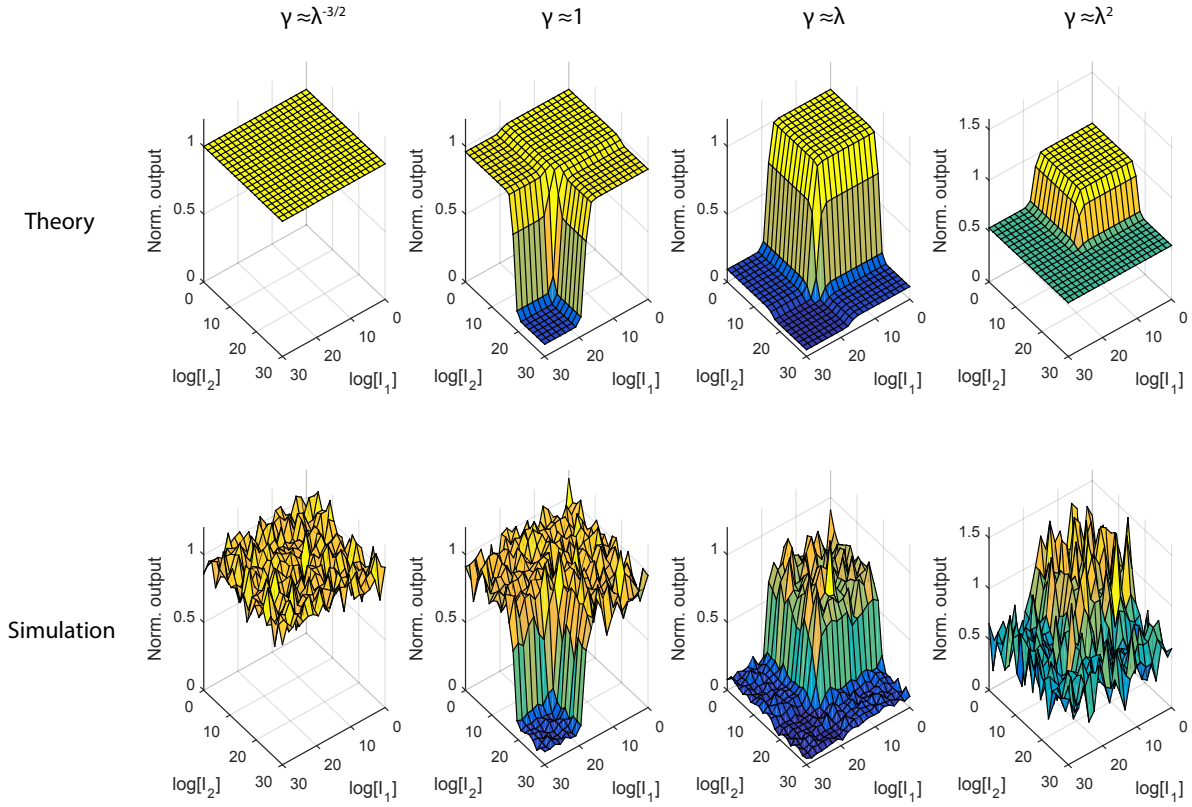

FIG. 7: Surface plots of gate output for the NAND gate with varying levels of promoter leakage, using deterministic theory (Eq. (7)) and stochastic simulations of the gate. The gate functionality shifts from FALSE, to NAND, to NOR, to noisy as the leakage increases. The parameters $\lambda_1 = \lambda_2 = \lambda_3 = \lambda_4 = \lambda = 0.002$ and $\alpha = 21.8$ implying $\alpha \approx \lambda^{-1/2}$. Other parameter values are given in the methods. The log is base 10. Note that the y axis shows the gate output normalised by the deterministic maximum (color online).

III. DISCUSSION

In this article, we have used deterministic modelling to understand how the function of low-leakage genetic logic gates varies with the rate constants characterising the reactions at the heart of the gate. We have identified simple power law relationships between parameters which lead to specific gate functions and showed that even if leakage is practically negligible, still a network can display logic function which is completely different than the one suggested by the network's connectivity. The main results of our findings are summarised in Tables III and VI. Our findings are consistent with those found regarding network motifs not involved

in genetic logic gates [28] namely that network connectivity is not by itself sufficient to determine function.

Previous studies [29, 30] have shown that the truth table of the classic (wild type) lacZYA operon of *Escherichia coli* (as a function of its two inducers, cAMP and IPTG) is intermediate between that of an AND gate and an OR gate. It was also shown that mutations can result in purer AND-like or OR-like functions. Our results are in broad agreement with the latter, in particular verifying that the plasticity of the truth table is not a property of just naturally occurring biochemical systems but it is also shared by purposefully designed synthetic genetic logic gates. An interesting observation is that the optimal AND gate function obtained in our synthetic AND gate has a much sharper switching threshold than the same optimal AND gate function obtained by a mutation of the lacZYA operon (compare the case $\gamma = \lambda^{1/2}$ in Fig. 4 in this paper with Fig. 5b in the paper [29]). We note that in contrast to previous studies, our study determines the non-trivial mathematical relationship between parameters leading to a desired optimal logic gate function.

Good agreement of deterministic theory with stochastic simulations using the Gillespie algorithm show that the logic gate function is robust to intrinsic noise, i.e fluctuations in the molecule numbers stemming from uncertainty in the time between successive reactions and which reaction fires next. This means that if there is little cell-to-cell variation in a population of cells, i.e. parameter values for the gates are essentially the same for all cells, then each cell will display the same logic gate behaviour. However if there is significant variation in the parameters between cells then because of the sensitivity of logic gate behaviour to parameter values, one might have some cells displaying one logic gate function whilst others displaying a second one.

A criticism of our study would be that it is conducted in steady-state conditions while cells are constantly growing, dividing and adapting to their environmental conditions. It has been recently shown that for various cell types, an approximate constancy in gene product concentration is achieved, independent of cell size and hence of the cell cycle, by means of size-dependent expression or scaling of gene dosage with size [31]. Hence our enforcement of steady-state conditions can be seen as a rough approximation to the intracellular concentration homeostasis enforced by various mechanisms. It is difficult to further increase the predictive power of the model without specifying a particular cell type. A more detailed stochastic study incorporating homeostatic mechanisms, gene replication, cell growth, par-

titioning of proteins at cell division, and details of the cell cycle specific to a particular cell type will be needed to make accurate predictions on the robustness and function of genetic logic gates in living cells.

IV. METHODS

A. AND Gate

The AND gate - with inputs I_1, I_2 and output R_3 as illustrated in Fig. 1 - is defined by the following chemical reaction network:

$$P_1 \underset{a_1'}{\overset{a_1[I_1]}{\rightleftharpoons}} P_1^\star,\ P_1^\star \xrightarrow{t_1} P_1^\star + R_1,\ R_1 \xrightarrow{d_1} \emptyset,\ P_2 \underset{a_2'}{\overset{a_2[I_2]}{\rightleftharpoons}} P_2^\star,\ P_2^\star \xrightarrow{t_2} P_2^\star + R_2,\ R_2 \xrightarrow{d_2} \emptyset, \qquad (12)$$
$$R_1 + R_2 \underset{k_b}{\overset{k_f}{\rightleftharpoons}} R_{12},\ P_3 + R_{12} \underset{a_3'}{\overset{a_3}{\rightleftharpoons}} P_3^\star,\ P_3^\star \xrightarrow{t_3} P_3^\star + R_3,\ R_3 \xrightarrow{d_3} \emptyset$$

where $a_i,\ a_i'$ are the association and dissociation rates respectively for P_i; $t_i,\ d_i$ are the transcription and degradation rates respectively for R_i and $k_f,\ k_b$ are the association and dissociation rates for the R_{12} complex. In these reactions we have neglected promoter leakage; if we take this into account, the new reaction scheme reads:

$$P_1 \underset{a_1'}{\overset{a_1[I_1]}{\rightleftharpoons}} P_1^\star,\ \emptyset \underset{d_1}{\overset{l_1 n_1/V}{\rightleftharpoons}} R_1,\ P_1^\star \xrightarrow{t_1} P_1^\star + R_1,\ P_2 \underset{a_2'}{\overset{a_2[I_2]}{\rightleftharpoons}} P_2^\star,\ \emptyset \underset{d_2}{\overset{l_2 n_2/V}{\rightleftharpoons}} R_2,\ P_2^\star \xrightarrow{t_2} P_2^\star + R_2, \qquad (13)$$
$$R_1 + R_2 \underset{k_b}{\overset{k_f}{\rightleftharpoons}} R_{12},\ P_3 + R_{12} \underset{a_3'}{\overset{a_3}{\rightleftharpoons}} P_3^\star,\ \emptyset \underset{d_3}{\overset{l_3 n_3/V}{\rightleftharpoons}} R_3,\ P_3^\star \xrightarrow{t_3} P_3^\star + R_3,$$

where l_i are the leakage rates respectively for R_i, n_i is the total promoter number of P_i, V is the cell volume and all other constants are as before. Since the zero leakage case (12) is a special case of (13) we shall study in detail the latter. The REs for the concentrations of

the species of reaction scheme (13) are:

$$\begin{aligned}
\partial_t [P_1^\star] &= a_1 [I_1] (n_1/V - [P_1^\star]) - a_1' [P_1^\star], \\
\partial_t [P_2^\star] &= a_2 [I_2] (n_2/V - [P_2^\star]) - a_2' [P_2^\star], \\
\partial_t [P_3^\star] &= a_3 [R_{12}] (n_3/V - [P_3^\star]) - a_3' [P_3^\star], \\
\partial_t [R_1] &= l_1 n_1/V - d_1 [R_1] + t_1 [P_1^\star] - k_f [R_1] [R_2] + k_b [R_{12}], \\
\partial_t [R_2] &= l_2 n_2/V - d_2 [R_2] + t_2 [P_2^\star] - k_f [R_1] [R_2] + k_b [R_{12}], \\
\partial_t [R_{12}] &= k_f [R_1] [R_2] - k_b [R_{12}] - a_3 [R_{12}] (n_3/V - [P_3^\star]) + a_3' [P_3^\star], \\
\partial_t [R_3] &= l_3 n_3/V - d_3 [R_3] + t_3 [P_3^\star].
\end{aligned} \tag{14}$$

At steady-state, we find that:

$$[R_3] = C_3 \left(\lambda_3 + \frac{C_1 C_2 \left(\lambda_1 + \frac{[I_1]}{[I_1]+K_1}\right)\left(\lambda_2 + \frac{[I_2]}{[I_2]+K_2}\right)}{K_3 K_{12} + C_1 C_2 \left(\lambda_1 + \frac{[I_1]}{[I_1]+K_1}\right)\left(\lambda_2 + \frac{[I_2]}{[I_2]+K_2}\right)} \right), \tag{15}$$

where $C_i = \frac{t_i n_i}{V d_i}$ is the maximum concentration of R_i (without leakage), $K_i = \frac{a_i'}{a_i}$ is the dissociation constant for P_i, $K_{12} = \frac{k_b}{k_f}$ is the dissociation constant for R_{12}, and $\lambda_i = \frac{l_i}{t_i}$ is the relative leakage of promoter P_i.

B. NAND Gate

The NAND gate - with inputs I_1, I_2 and output R_4 - is defined by the following chemical reaction network, in addition to those in Eq. (13):

$$P_4 \underset{a_4'}{\overset{a_4}{\rightleftharpoons}} P_4^\star + R_3, \ \emptyset \underset{d_4}{\overset{l_4 n_4/V}{\rightleftharpoons}} R_4, \ P_4^\star \xrightarrow{t_4} P_4^\star + R_4, \tag{16}$$

where $a_4,\ a_4',\ d_4,\ t_4,\ l_4$ and n_4 are defined analogously to Eq. (13). The ODEs for all species except $[R_3]$ are the same as in Eq. (14). The ODEs for $[R_3]$, $[R_4]$ and $[P_4^\star]$ are given by:

$$\begin{aligned}
\partial_t [P_4^\star] &= a_4 (n_4/V - [P_4^\star]) - a_4' [R_3] [P_4^\star], \\
\partial_t [R_3] &= l_3 n_3/V - d_3 [R_3] + t_3 [P_3^\star] + a_4 (n_4/V - [P_4^\star]) - a_4' [R_3] [P_4^\star], \\
\partial_t [R_4] &= l_4 n_4/V - d_4 [R_4] + t_4 [P_4^\star].
\end{aligned} \tag{17}$$

At steady-state, we find that:

$$[R_4] = C_4 \left(\lambda_4 + K_4 \left[K_4 + C_3 \left(\lambda_3 + \frac{C_1 C_2 \left(\lambda_1 + \frac{I_1}{I_1+K_1}\right)\left(\lambda_2 + \frac{I_2}{I_2+K_2}\right)}{K_3 K_{12} + C_1 C_2 \left(\lambda_1 + \frac{I_1}{I_1+K_1}\right)\left(\lambda_2 + \frac{I_2}{I_2+K_2}\right)} \right) \right]^{-1} \right), \tag{18}$$

where $C_4 = \frac{t_4 n_4}{V d_4}$, $K_4 = \frac{a_4}{a'_4}$, and $\lambda_4 = \frac{l_4}{t_4}$.

C. Stochastic simulations

Stochastic simulations were performed using the Gillespie algorithm [21]. Each point in the stochastic plots in Figs. 4 and 7 shows an independent simulation at 100 seconds into steady-state simulation.

Parameter values used in Figs. 4 and 7 were taken from experimentally-determined ranges: $a_1 = a_2 = a_3 = a'_4 = a = 4.8 \times 10^{-20} m^3 s^{-1}$ [32], $a'_1 = a'_2 = a'_3 = a_4 = a' = 2.2 s^{-1}$ [33], $n_i = n = 1$, $V = 3 \times 10^{-19} m^3$ [34], $t_i = t = 3.0 s^{-1}$ [35], $d_i = d = 10^{-2} s^{-1}$ [35] (for all i), $k_f = 1.7 \times 10^{-22} m^3 s^{-1}$ [35] and $\lambda = 0.002$. In order to vary γ, k_b is varied according to the formula $k_b = \frac{\gamma t^2 n^2 a k_f}{V^2 a' d^2}$ (which follows from the definition of γ).

V. ACKNOWLEDGEMENTS

The authors would like to thank Baojun Wang and Xinyi Wan for useful discussions. This work was funded by a BBSRC EASTBIO PhD studentship to S.S.

[1] W. A. Lim, Nature reviews Molecular cell biology **11**, 393 (2010).

[2] B. Wang, R. I. Kitney, N. Joly, and M. Buck, Nature communications **2**, 508 (2011).

[3] A. Hofmann, J. Falk, T. Prangemeier, D. Happel, A. Köber, A. Christmann, H. Koeppl, and H. Kolmar, Nucleic Acids Research (2018).

[4] N. Joshi, X. Wang, L. Montgomery, A. Elfick, and C. French, Desalination **248**, 517 (2009).

[5] N. Saeidi, C. K. Wong, T.-M. Lo, H. X. Nguyen, H. Ling, S. S. J. Leong, C. L. Poh, and M. W. Chang, Molecular systems biology **7**, 521 (2011).

[6] T. S. Moon, C. Lou, A. Tamsir, B. C. Stanton, and C. A. Voigt, Nature **491**, 249 (2012).

[7] J. J. Tabor, H. M. Salis, Z. B. Simpson, A. A. Chevalier, A. Levskaya, E. M. Marcotte, C. A. Voigt, and A. D. Ellington, Cell **137**, 1272 (2009).

[8] J. A. Brophy and C. A. Voigt, Nature methods **11**, 508 (2014).

[9] K. I. Ramalingam, J. R. Tomshine, J. A. Maynard, and Y. N. Kaznessis, Biochemical Engineering Journal **47**, 38 (2009).

[10] M. A. Marchisio and J. Stelling, PLoS Comput Biol **7**, e1001083 (2011).

[11] D. Sanassy, H. Fellermann, N. Krasnogor, S. Konur, L. M. Mierla, M. Gheorghe, C. Ladroue, and S. Kalvala, in *High Performance Computing and Communications, 2014 IEEE 6th Intl Symp on Cyberspace Safety and Security, 2014 IEEE 11th Intl Conf on Embedded Software and Syst (HPCC, CSS, ICESS), 2014 IEEE Intl Conf on* (IEEE, 2014), pp. 404–408.

[12] D. Soloveichik, M. Cook, E. Winfree, and J. Bruck, natural computing **7**, 615 (2008).

[13] M. Gerstung, J. Timmer, and C. Fleck, Physical Review E **79**, 011923 (2009).

[14] H. Ando, S. Sinha, R. Storni, and K. Aihara, EPL (Europhysics Letters) **93**, 50001 (2011).

[15] A. Dari, B. Kia, X. Wang, A. R. Bulsara, and W. Ditto, Physical Review E **83**, 041909 (2011).

[16] A. Goñi-Moreno and M. Amos, BMC systems biology **6**, 126 (2012).

[17] L. Huang, Z. Yuan, P. Liu, and T. Zhou, BMC systems biology **9**, 16 (2015).

[18] J. M. Callura, C. R. Cantor, and J. J. Collins, Proceedings of the National Academy of Sciences p. 201203808 (2012).

[19] P. Siuti, J. Yazbek, and T. K. Lu, Nature biotechnology **31**, 448 (2013).

[20] E. Klipp, R. Herwig, A. Kowald, C. Wierling, and H. Lehrach, *Systems biology in practice: concepts, implementation and application* (John Wiley & Sons, 2008).

[21] D. T. Gillespie, The journal of physical chemistry **81**, 2340 (1977).

[22] H. Enderton and H. B. Enderton, *A mathematical introduction to logic* (Academic press, 2001).

[23] D. Schnoerr, G. Sanguinetti, and R. Grima, Journal of Physics A: Mathematical and Theoretical **50**, 093001 (2017).

[24] R. Grima, The Journal of chemical physics **133**, 07B604 (2010).

[25] R. Grima, The Journal of chemical physics **136**, 04B616 (2012).

[26] A. Bar-Even, E. Noor, Y. Savir, W. Liebermeister, D. Davidi, D. S. Tawfik, and R. Milo, Biochemistry **50**, 4402 (2011).

[27] L. Arike, K. Valgepea, L. Peil, R. Nahku, K. Adamberg, and R. Vilu, Journal of proteomics **75**, 5437 (2012).

[28] P. J. Ingram, M. P. Stumpf, and J. Stark, BMC genomics **7**, 108 (2006).

[29] Y. Setty, A. E. Mayo, M. G. Surette, and U. Alon, Proceedings of the National Academy of Sciences **100**, 7702 (2003).

[30] A. E. Mayo, Y. Setty, S. Shavit, A. Zaslaver, and U. Alon, PLoS biology **4**, e45 (2006).

[31] C. A. Vargas-Garcia, K. R. Ghusinga, and A. Singh, Current opinion in systems biology (2018).

[32] H. C. Nelson and R. T. Sauer, Cell **42**, 549 (1985).

[33] D. Van Valen, D. Wu, Y.-J. Chen, H. Tuson, P. Wiggins, and R. Phillips, Current Biology **22**, 1339 (2012).

[34] H. Kubitschek, Journal of bacteriology **172**, 94 (1990).

[35] D. Toner and R. Grima, Scientific reports **3**, 2438 (2013).